Ice-nucleating particle emissions from biomass combustion and the potential importance of soot aerosol

E. J.T. Levin
Colorado State University

G. R. McMeeking
Colorado State University

P. J. DeMott
Colorado State University

C. S. McCluskey
Colorado State University

C. M. Carrico
New Mexico Institute of Mining and Technology

Recommended Citation

Levin, E. J.T.; McMeeking, G. R.; DeMott, P. J.; McCluskey, C. S.; Carrico, C. M.; Nakao, S.; Jayarathne, T.; Stone, E. A.; Stockwell, C. E.; Yokelson, R. J.; and Kreidenweis, S. M., "Ice-nucleating particle emissions from biomass combustion and the potential importance of soot aerosol" (2016). *Chemistry and Biochemistry Faculty Publications*. 126.
https://scholarworks.umt.edu/chem_pubs/126

Authors

E. J.T. Levin, G. R. McMeeking, P. J. DeMott, C. S. McCluskey, C. M. Carrico, S. Nakao, T. Jayarathne, E. A. Stone, C. E. Stockwell, R. J. Yokelson, and S. M. Kreidenweis

RESEARCH ARTICLE

Key Points:
- Fires emit ice-nucleating particles
- Black carbon contributes to the INPs emitted from fires
- Fire emissions have lower ice-nucleating efficiency than other sources

Ice-nucleating particle emissions from biomass combustion and the potential importance of soot aerosol

E. J. T. Levin[1], G. R. McMeeking[1,2], P. J. DeMott[1], C. S. McCluskey[1], C. M. Carrico[3], S. Nakao[1,4], T. Jayarathne[5], E. A. Stone[5], C. E. Stockwell[6], R. J. Yokelson[6], and S. M. Kreidenweis[1]

[1]Department of Atmospheric Science, Colorado State University, Fort Collins, Colorado, USA, [2]Now at Handix Scientific, Boulder, Colorado, USA, [3]Department of Civil and Environmental Engineering, New Mexico Institute of Mining and Technology, Socorro, New Mexico, USA, [4]Now at Department of Chemical and Biomolecular Engineering, Clarkson University, Potsdam, New York, USA, [5]Department of Chemistry, University of Iowa, Iowa City, Iowa, USA, [6]Department of Chemistry, University of Montana, Missoula, Montana, USA

Abstract Ice-nucleating particles (INPs) are required for initial ice crystal formation in clouds at temperatures warmer than about −36°C and thus play a crucial role in cloud and precipitation formation. Biomass burning has been found to be a source of INPs in previous studies and is also a major contributor to atmospheric black carbon (BC) concentrations. This study focuses on isolating the BC contribution to the INP population associated with biomass combustion. Emissions of condensation mode INPs from a number of globally relevant biomass fuels were measured at −30°C and above water saturation as fires progressed from ignition to extinguishment in a laboratory setting. Number emissions of INPs were found to be highest during intense flaming combustion (modified combustion efficiency > 0.95). Overall, combustion emissions from 13 of 22 different biomass fuel types produced measurable INP concentrations for at least one replicate experiment. On average, all burns that produced measureable INPs had higher combustion efficiency, which is associated with higher BC emissions, than those that did not produce measureable INPs. Across all burns that produced measureable INPs, concentrations ranged from 0.1 to 10 cm^{-3}, and the median emission factor was about 2×10^7 INPs per kilogram of fuel burned. For a subset of the burns, the contribution of refractory black carbon (rBC) to INP concentrations was determined by removing rBC via laser-induced incandescence. Reductions in INPs of 0–70% were observed, indicating an important contribution of rBC particles to INP concentrations for some burns, especially marsh grasses.

1. Introduction

Ice-nucleating particles (INPs) possess the ability to initiate ice crystal formation in clouds at temperatures warmer than about −36°C [*DeMott et al.*, 2010]. These unique particles, therefore, play an important role in ice crystal formation in clouds and can affect cloud lifetimes and optical properties as well as precipitation formation [*Lu and Sokolik*, 2013; *Sassen and Khvorostyanov*, 2008]. Understanding what types of aerosol particles are capable of initiating ice crystal formation, as well as their sources, is crucial for our ability to understand and model clouds and precipitation. However, despite their importance, there is still uncertainty about what types of particles are capable of acting as ice crystal nuclei in clouds [*Levin and Cotton*, 2009]. Further, the various sources and classes of INPs and their abundance in the atmosphere are also not fully characterized.

Combustion sources are potential emitters of INPs to the atmosphere. For example, *DeMott* [1990] and *Diehl and Mitra* [1998] measured kerosene soot at −20 to −22°C and found that as many as 1 in 1000 of the particles initiated immersion freezing at these temperatures. Using these data, *Murray et al.* [2012] estimated that soot could be as important as dust in a global, annually averaged, INP inventory. *Umo et al.* [2015] performed immersion freezing experiments on bottom ash, the mineral material left behind after combustion. While these particles are much more similar to dust than carbonaceous aerosol, they found INP activities slightly lower than desert dusts. Biomass combustion, such as wildfires, prescribed burning, and agricultural burning, has also been shown to be a potential source of INPs to the atmosphere. *Prenni et al.* [2012] and *McCluskey et al.* [2014] measured INP concentrations downwind of both prescribed burns and wildfires and observed increases in INP concentrations when the measurement site was impacted by smoke plumes, especially during times when the fire was visually dominated by flaming combustion. *Twohy et al.* [2010] also found highest measured INP

concentrations during an aircraft study when sampling in a prescribed fire plume and also observed positive correlations between black carbon (BC) aerosol and both ice crystal and INP number concentrations within orographic clouds. Further, *Sassen and Khvorostyanov* [2008] remotely observed impacts on ice cloud formation due to smoke from wildfires. Laboratory measurements of biomass combustion smoke have also shown increases in INP concentrations for some experimental burns, although other burns produced no measurable increase in INP concentrations [*Petters et al.*, 2009].

Globally, open biomass combustion is estimated to emit 2700 Gg of BC aerosol annually, accounting for roughly one third of total BC emissions [*Bond et al.*, 2013]. These BC particles are insoluble in water and have complex fractal geometry, both favorable qualities for heterogeneous ice nucleation [*Hoose and Moehler*, 2012], and have been suggested as a potential INP type [*Gorbunov et al.*, 2001; *Murray et al.*, 2012; *Twohy et al.*, 2010]. However, fires are also highly complex systems emitting a diverse range of aerosols with variable size, mixing state, and chemical composition [*Reid et al.*, 2005]. Further, INPs represent a small fraction of total emitted particles, making it hard to correlate with bulk fire properties. Thus, the increases in INP concentrations from fires cannot be attributed to specific particle types without further analysis. *McCluskey et al.* [2014] performed such an analysis by collecting ice crystals nucleated in smoke samples and then examining the residual particles via electron microscopy. When measuring in smoke plumes, they observed INP compositions containing both carbonaceous and noncarbonaceous particles. For some cases soot accounted for up to two thirds of the analyzed ice crystal residuals. This time-consuming method cannot be performed in real time, however, and offers only a small snapshot of residual INPs.

To better constrain INP emission from biomass combustion, a series of burns were conducted during the fourth Fire Laboratory at Missoula Experiment (FLAME 4). The first set of burn experiments were designed to allow for characterization of INP emissions in real time as the fires progressed through ignition, flaming, smoldering, and extinction stages. To our knowledge this is the first time such measurements have been made in a semicontrolled laboratory setting. *Petters et al.* [2009] measured burn integrated INP emissions from laboratory fires mixed in a large tank. While they were able to classify the relative contribution of emissions from flaming versus smoldering combustion using modified combustion efficiency (MCE), they were not able to measure these emissions separately as the fire conditions changed. *Prenni et al.* [2012] and *McCluskey et al.* [2014], who measured smoke from prescribed burns and wildfires, were only able to qualitatively determine the level of flaming versus smoldering combustion visually. These studies were also performed at variable distances from the fire, so that smoke age was not constant and was not quantified.

During the second phase of FLAME 4 we conducted experiments on burn integrated emissions with extended sampling times, up to 4 h. This allowed time to employ the new technique presented by *Levin et al.* [2014] and *Aiken et al.* [2016] to remove refractory black carbon (rBC) particles from the sample via laser-induced incandescence and vaporization. By measuring INP concentrations with and without the rBC component of the smoke, we were able to directly determine the contribution of these carbonaceous particles to the INP population for select biomass fuels.

2. Methods

2.1. FLAME 4 Setup and Fuels

The FLAME 4 study was conducted at the U.S. Forest Service Fire Sciences Laboratory in Missoula, MT, during October and November, 2012 [*Stockwell et al.*, 2014]. The combustion facility consists of a large (~3500 m^3) combustion lab with a 1.6 m diameter exhaust stack in the middle extending from the ceiling down to ~2 m above the floor [*McMeeking et al.*, 2009; *Yokelson et al.*, 2008]. Instruments can be placed on a platform that surrounds the stack at a height of 17 m above the floor where fire emissions can be measured directly from the stack. Instrumentation can also be placed in adjacent labs with sampling ports into the combustion lab. The fuels burned during FLAME 4, discussed in detail by *Stockwell et al.* [2014], represented a range of globally relevant fuels commonly consumed during prescribed burns, clearing of agricultural fields, and wildfires. As well as biomass fuels, burn experiments were also conducted with shredded tires, plastic bags, and trash, and emissions from a number of cook stoves were also investigated. For this work we focus on the open biomass combustion experiments.
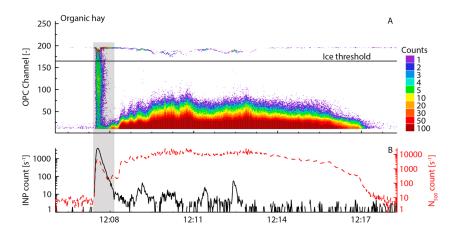
Figure 1. Example OPC output for an organic hay burn. (a) A contour plot of raw OPC output, with red colors indicating higher counts. The black line is the ice threshold size. (b) Summed INP counts (solid black line) and total counts above 500 nm (dashed red line) per second. The shaded area shows the time period affected by the match that was used to ignite this burn, and these data were removed from final analysis.

Two types of experiments were performed during FLAME 4. During "stack" burns, fires were lit directly below the exhaust stack, while instrumentation was placed on the platform near the top of the stack. Sample was drawn from the middle of the stack through sampling ports to the instrumentation. Previous studies have shown that emissions are well mixed across the stack profile, and the average smoke age at the sampling height is about 5 s [*Christian et al.*, 2004]. Stack burns allowed for measurements to be made in real time as the fires progressed from ignition through flaming, smoldering, and extinction phases. Burns typically lasted only a few minutes, permitting many different burns to be performed over the course of the day. We were also able to perform multiple burns with the same fuel type and initial mass. However, due to the complexity of fire behavior, these should not be considered true experimental replicates.

For the second half of FLAME 4 we conducted "room" burns. For these experiments the combustion lab was sealed, including closing the exhaust stack; fires were lit on one side of the combustion lab, and smoke was held in the room for several hours. Most instrumentation was housed in a lab adjacent to the combustion lab, and sample was drawn through a line which extended to near the middle of the combustion lab at a height of ~2 m. During these experiments, we sampled burn-integrated emissions mixed in the combustion lab and thus could not distinguish between flaming and smoldering emissions other than determining relative contributions using combustion efficiency calculations. However, the room burns allowed for extended sampling periods, and thus, we could perform experiments that required more time and more stable aerosol concentrations.

For both stack and room burns, between 100 and 2000 g of fuel was placed on a ceramic fuel bed which was continuously weighed using two balances (Mettler-Toledo PM34). Burns were ignited using a resistive heating coil on the ceramic fuel bed or were lit with either a propane torch or a match. The heating coil caused the entire fuel bed to ignite simultaneously, while the other ignition methods were used to ignite one side of the fuel bed, allowing the flame front to propagate horizontally through the fuel. Each ignition method was tested separately to determine any influence on emissions of INPs. The match produced a large INP signal when first struck, as can been seen in Figure 1, and thus, for the few burns that used this ignition method the first few seconds of data were removed to ensure no contamination of the signal. No matches were used during the room burns when all fire emissions were mixed in the combustion lab and sampled together. The other ignition methods produced no measureable INP signals.

2.2. Instruments

We measured INP concentrations using the Colorado State University Continuous Flow Diffusion Chamber (CFDC), originally described by *Rogers* [1988], *Rogers et al.* [2001], and more recently by *DeMott et al.* [2015]. The instrument introduces a laminar sample flow into a temperature- and relative humidity-controlled growth region (comprising the upper two thirds of the chamber) with ice-coated walls (ice thickness ~0.1 mm). For this study, the CFDC was operated in a manner to initially grow liquid droplets on all particles which would then freeze if the particle was an INP at the processing temperature. Liquid droplets were

evaporated in the lower one third of the chamber, while ice crystals remained, prior to detection of exiting aerosols and ice particles with an optical detector. For this study, residence time in the growth region of the CFDC was 4.8 s, and target conditions for sampled particles in this region were typically set as $T = -30°C$ and relative humidity (RH) = 105% or 5% supersaturation with respect to water (S_w). During the room burns, some measurements were also made at $-28°C$ and $-32°C$. By operating the CFDC above water saturation, there is no ability to distinguish between condensation-freezing and immersion-freezing mode INPs. However, as pointed out by *Vali et al.* [2015], there is no strong existing evidence to consider that these modes access different INP populations. The optical particle counter (OPC; CLIMET 3100) distinguished ice crystals and non-INP aerosol based on diameter, using 3 μm as the ice crystal minimum size threshold. A 2.4 μm (50% diameter size cut) impactor on the CFDC inlet was used to remove any large aerosol from the sample, which could be mistakenly counted as activated INPs. Filtered air was measured regularly at the same processing conditions to determine background levels of false INP counts, which were subtracted from the sample aerosol signal. This measurement, along with the measured sample volume, gives the number concentrations of INPs (N_{INP}) as well as that of aerosol larger than the lower detection limit of the OPC, roughly 500 nm (N_{500}). As an example, Figure 1 shows the raw OPC counts for one burn binned into 256 size bins (Figure 1a) as well as the summed INP and aerosol counts above and below the ice threshold per second (Figure 1b). The large spike in both N_{INP} and N_{500} at the beginning of the burn was due to the match that was used to ignite this burn. This artifact response, due to unknown components in the match emissions acting as INPs, was removed from the final analysis.

During certain room burn experiments, a Single Particle Soot Photometer (SP2; Droplet Measurement Technologies) was used to remove refractory black carbon (rBC) particles upstream of the CFDC as described by *Levin et al.* [2014] and *Aiken et al.* [2016]. The SP2 uses a 1064 nm Nd:YAG laser to heat light-absorbing material, primarily rBC, larger than ~70 nm in spherical equivalent diameter, to its vaporization point, thus removing it from the sample [*Aiken et al.*, 2016]. By sampling downstream of the SP2 with the CFDC and cycling the SP2 laser power every 3 min, we were able to determine the contribution of rBC or rBC-containing particles to N_{INP} and N_{500} by taking the difference of unperturbed (laser off) and rBC-"free" (laser on) INP measurements. *Levin et al.* [2014] performed a number of tests on this setup to ensure that rBC particles were in fact removed from the sample and that laser processing did not lead to any changes in nonabsorbing aerosol particle concentrations. They found that SP2 laser processing did not affect the concentrations or size of purely light-scattering polystyrene latex test aerosol, while pure rBC samples were removed above a diameter of ~100 nm. When sampling rBC-containing aerosol, they observed the formation of a new aerosol mode at small diameters, < 70 nm, from either condensation of vaporized rBC or fragmentation of the original rBC particles [*Aiken et al.*, 2016]. These new particles had no effect on INP concentrations. The SP2 laser also had no effect on INP concentrations measured downstream for purely light-scattering kaolinite. However, the ice-nucleating ability of kaolinite internally mixed with rBC was affected by the SP2 laser processing.

For select experiments, ice crystals were collected via inertial impaction at the base of the CFDC for subsequent offline analysis of the ice-nucleating particles via scanning electron microscopy (SEM) with energy dispersive X-ray (EDX) capability, as described by *McCluskey et al.* [2014]. This analysis was done at the Materials Characterization Laboratory in the Department of Geology and Geophysics at the University of Wyoming (Laramie, WY). Images and elemental composition were then used to subjectively classify each analyzed INP as soot, soot containing, or other, nonsoot, aerosol.

As well as N_{INP} and N_{500}, a suite of other instruments were used to measure aerosol and gas emissions from the fires. Aerosol size distributions between 5.6 and 560 nm were measured with a Fast Mobility Particle Sizer (FMPS; TSI), which uses electrical mobility and an array of detectors to measure size distributions with 32 size bins at 1 Hz time resolution [*Levin et al.*, 2015]. We integrated the FMPS data below 500 nm and added N_{500} measured by the CFDC OPC to calculate N_{total}, which thus spanned the range 5.6 nm to 2.4 μm. An open-path Fourier transform infrared radiometer (OP-FTIR) was used to measure mixing ratios of CO, CO_2, and other trace gas species emitted during combustion [*Stockwell et al.*, 2014]. The OP-FTIR was placed on the measurement platform during both stack and room burns and operated with 1.5 s temporal resolution during stack burns and 6 s during room burns. Particulate matter < 2.5 μm in diameter was collected onto precleaned quartz-fiber filters which were subsequently analyzed thermo-optically for organic (OC) and elemental (EC) carbon mass concentrations using a Sunset

OC-EC aerosol analyzer (Sunset Laboratory) following the IMPROVE-A temperature ramping protocol [*Chow et al.*, 2007]. We calculated total aerosol carbon mass (TC) as the sum of EC and OC. Aerosol scattering (b_{scat}) and absorption (b_{abs}) coefficients at 870 nm were measured with a photoacoustic extinctiometer (PAX 870; Droplet Measurement Technologies) [*Arnott et al.*, 1999; *Nakayama et al.*, 2015]. We used these measurements to calculate single scattering albedo (SSA) via

$$SSA = \frac{b_{scat}}{b_{scat} + b_{abs}} \tag{1}$$

We note that in the above instrument descriptions the terms "EC," "BC," "rBC," and "soot" are all measurement-specific and not necessarily interchangeable [*Petzold et al.*, 2013]. While we use these terms as appropriate when discussing the different measurement results, for our analysis we assume that all these measurements are probing the same carbonaceous component of the emitted aerosol.

2.3. Data Processing

The OPC at the base of the CFDC generated 1 Hz particle counts, which we binned into 256 bins, as shown in Figure 1. We integrated the counts above the bins corresponding to diameters of 0.5 and 3 µm, respectively, to produce aerosol and INP counts (Figure 1). We then used the measured sample flow rate to calculate N_{500} and N_{INP} and then averaged to a 5 s running mean. Instrument background, measured counts resulting from frost flaking off of the inner surface of the instrument, was determined by measuring high-efficiency particulate air (HEPA) filtered air before and after each stack burn and repeatedly at intervals during every room burn. These time periods were averaged, and a linear fit between two consecutive filter measurements was subtracted from the data to remove the effect of these counts. Further, we only report INP data that are statistically significantly different from the filter background measurements at the 95% confidence level. Room background was also measured by sampling for a few minutes before each burn and was subtracted from the burn data in the same way as the filter measurements. Both room and filter background values were typically < 10% of the values measured during burns.

Correction of the CFDC INP data was necessitated due to the very high total aerosol concentrations emitted from the fires and sampled during FLAME 4 (average N_{total} across all stack burns was 2.39×10^6 cm^{-3}). Calculations, laboratory experiments, and analysis of this and other data sets, all detailed in the supporting information, showed that water vapor in the CFDC was depleted under these aerosol conditions due to consumption by activating and growing droplets, leading to a lower RH in the growth region of the CFDC than the targeted values [*Rogers*, 1988]. The decreased RH could have prevented condensation/immersion mode INP from effectively activating by limiting water uptake and activation of the entire aerosol population as droplets, thus leading to an underestimation of N_{INP}. Previous experiments have shown that N_{INP} measured by the CFDC is highly sensitive to the processing RH at modest values above water saturation [*DeMott et al.*, 2015; *Petters et al.*, 2009]. While it is also possible that the decrease in processing RH led to activation of some INPs at water subsaturated conditions, measurements made specifically below water saturation, but still above ice saturation, showed no observable ice crystal formation. If ice crystals were nucleated at these conditions, they would grow to detectable sizes as the presence of high number concentrations of unactivated aerosols would not limit ice supersaturation. Thus, we assume that all measured INPs were activated in the immersion mode.

To correct the FLAME 4 data for any potential undercounting, we fit a single curve to seven data sets spanning more than 4 orders of magnitude of N_{total} and used this fit to adjust the measured INP concentrations (see supporting information). Below we will present N_{INP} values as measured directly as well as those corrected using this method to show the potential undercounting due to vapor limitation effects in the CFDC during FLAME 4. Further, these results have implications for all high particle concentration measurement scenarios using the Colorado State University CFDC or similar instruments, such as those presented by *Prenni et al.* [2012] and *McCluskey et al.* [2014]. In ambient conditions with aerosol concentrations below about 1×10^4 cm^{-3}, undercounting due to vapor depletion should be no more than ~10%. When sampling in highly polluted environments or laboratory studies with high aerosol loadings, however, some dilution system could be considered to avoid potential undercounting of INPs. We chose not to dilute during FLAME 4 in order to better sample real-time behavior and to minimize any artifact due to perturbing the gas particle partitioning.
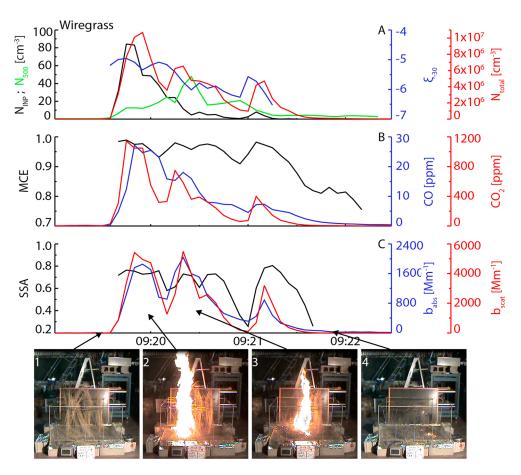
Figure 2. Example time lines of emitted aerosol and gas concentrations and properties for a wiregrass stack burn.

3. Results and Discussion

3.1. Stack Burns

The main questions we wished to address during the stack burns were the following: (1) which fuels, if any, produced INPs when burned? and (2) if burns did emit INPs, under what burning conditions were they emitted? To address these questions, during the stack phase of FLAME 4 we conducted 106 burns. Due to instrument operating requirements, we were able to sample with the CFDC for half of these burns (53), capturing 15 different fuel types. Burns either were missed due to high instrument background or were skipped intentionally to prepare the CFDC for later sampling or when a particular burn was specifically configured for other experimental groups and was not conducive to CFDC measurements.

To aid our analysis, we define ice nucleation efficiency at a given temperature T (ξ_T) as

$$\xi_T = \log_{10} \frac{N_{\text{INP}}}{N_{\text{Total}}} \qquad (2)$$

following *Petters et al.* [2009]. An example time line showing the evolution of aerosol concentrations (N_{INP}, N_{500}, N_{total}), ξ_{-30}, gas concentrations (CO and CO_2), and aerosol optical properties (b_{abs}, b_{scat}, SSA) for one burn is shown in Figure 2. Values of N_{INP} and ξ_{-30} are corrected for vapor depletion. Four images of the burn are also shown during the preburn (image 1), flaming (images 2 and 3), and smoldering (image 4) phases. Figure 2 also shows the calculated values of modified combustion efficiency (MCE), defined as

$$\text{MCE} = \frac{CO_2}{CO_2 + CO} \qquad (3)$$

Modified combustion efficiency indicates the relative contribution of flaming versus smoldering combustion to the fire emissions [*McMeeking et al.*, 2009; *Yokelson et al.*, 2008]. During incomplete combustion, carbon in the fuel is not fully oxidized and emissions contain a higher fraction of CO. Further, aerosol emissions from

Table 1. All Biomass Fuels Tested During the FLAME 4 Stack and Room Burns and Number of Burns That Did or Did Not Produce Measureable INP Concentrations

	Burns With Detectable INPs	Burns Without Detectable INPs
Stack		
African grass (tall)	6	0
Rice straw	6	0
Organic hay	6	0
Sawgrass	5	0
Giant cutgrass	4	0
Organic wheat straw	2	0
Sugarcane	2	0
Alfalfa	1	0
Manzanita	1	0
Wiregrass	4	2
African grass (short)	2	1
Canadian peat	0	1
Wheat straw	0	2
Chamise	0	3
Ponderosa pine[a]	0	5
Room		
Ponderosa pine	3	0
Organic hay	2	0
Wiregrass	2	0
Giant cutgrass	2	0
Organic wheat straw	1	0
Rice straw	1	0
Manzanita	1	0
Sawgrass	1	0
African grass (tall)	1	0
Black spruce	1	0
Sugarcane	1	0
Canadian peat	0	1

[a]Smoldering only.

smoldering combustion tend to have a higher fractional concentration of organic carbon, while flaming combustion emits more BC aerosol [*Levin et al.*, 2010]. Typically, MCE values greater than 0.9 are considered to indicate $> \sim 50\%$ flaming combustion, while lower values indicate that smoldering combustion is more dominant [*Yokelson et al.*, 2008]. The high MCE values measured during the majority of the burn shown in Figure 2 are indicative of intense flaming combustion, which is confirmed by the images taken of the burn. Only at the end of the burn did smoldering combustion become dominant.

The fuel for the burn shown in Figure 2 was 110 g of wiregrass, a plant species common to the southeastern coastal plain of the U.S. and subject to prescribed burns for land management purposes. The fuel was arranged vertically, using a wire screen to hold it in place, and the fire was lit from one edge, allowing the flame front to propagate through the standing fuel as would happen in a natural burn. This burn configuration resulted in three periods of more intense flaming combustion, two of which are shown in images 2 and 3.

While all three intense flaming events resulted in increases in both aerosol and gas concentrations, there was a large spike in total aerosol emissions during the first event, which also had the largest and most intense flames. Emissions of INPs followed a similar trend with a spike at the beginning of the burn that steadily decreased. Ice nucleation efficiency (ξ_{-30}) also decreased as the burn progressed, dropping from -5 to -6 with only a smaller increase during the second and third flaming events. There were no measureable INP emissions during the smoldering phase of the burn, indicated by the drop in MCE at the end of the burn and seen visibly in image 4. This pattern of peak N_{INP} occurring at the beginning of the burn, during the period of intense flaming combustion, was typical across all stack burn experiments. On average, peak INP concentrations occurred within the first minute of the burn, with burns lasting, from ignition to the termination of any measureable smoke emissions, about 4 min on average.

Across all of the fuel types tested during the stack burns, 11 produced measureable N_{INP} during at least one burn experiment with that fuel type. Table 1 lists all fuel types measured with the CFDC during the stack burns showing both the number of burns that emitted measureable N_{INP} and those with no measureable increase in N_{INP}. Four fuel types did not produce any measureable N_{INP} during any of the tested burns, while two fuels, wiregrass and another grass collected from Kruger National Park in South Africa, had burns both with and without measurable INP emissions. While we did not measure INP emissions from the Ponderosa pine stack burns, we were only able to sample during the smoldering phase of combustion for these cases.

To investigate potential differences between burns with and without measureable N_{INP}, we compared N_{total}, MCE, b_{abs}, and EC to TC ratio (EC/TC) averaged over the burns that did or did not produce measureable N_{INP} as shown in Table 1. We included b_{abs} in this analysis as this parameter is indicative of the number concentration of black carbon particles in the emissions, although it is also a function of particle size and mixing state, and,
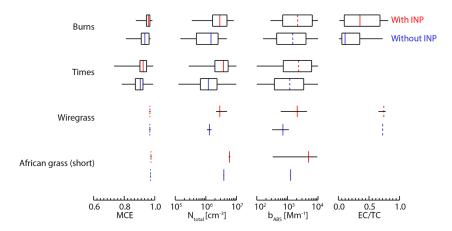
Figure 3. Values of N_{total}, MCE, b_{abs}, and EC/TC for (first row) burns that did (red) or did not (blue) produce INPs, (second row) time periods when INPs were or were not measured, and (third and fourth rows) for just wiregrass and short African grass burns. Boxes indicate 25th–75th percentiles, whiskers show minimum and maximum, and colored bars show median values. Solid median lines indicate that values were statistically significantly different at the 95% confidence level.

unlike the bulk filter measurements, b_{abs} was time resolved. Filter measurements were not available for 15 of the burns which produced INPs (38%) and 3 of those that did not (21%). The burns that did not produce measureable N_{INP} had lower median values of MCE, N_{total}, b_{abs}, and EC/TC (Figure 3). The differences in N_{total}, MCE, and EC/TC between burns that did and did not produce measureable N_{INP} were all statistically significantly different at the 95% confidence level using a two-tailed t test (represented by solid median lines in Figure 3). The difference in b_{abs} was only significant at an 85% confidence level.

Wiregrass and short African grass were unique in that these fuels had cases that both did and did not produce measureable N_{INP}. Again, although these burns used the same fuels, these should not be considered strict replicates due to the complex nature of fire behavior. Figure 3 also shows the minimum, maximum, and median N_{total}, MCE, b_{abs}, and EC/TC for the burns of these fuels which did and did not produce N_{INP}. Filter measurements were not available for the African grass burns. Unlike the differences across all fuel types, when only considering a single fuel type there were no differences in MCE or EC/TC for wiregrass, indicating that similar fuels burned in a similar fashion. However, the burns that had measureable increases in N_{INP} also had higher N_{total} and emitted a higher concentration of BC aerosol, as seen by the higher b_{abs} values. For both fuel types these differences were significant at a 95% confidence level. Given the higher concentration of aerosol emitted, it is possible that for the burns that did not have measureable N_{INP}, the INP levels were too low to be detected. That is, it is possible that the only important factor in whether or not a burn produced measureable N_{INP} was simply the amount of material emitted by the burn. We tested this hypothesis by calculating the ξ_{-30} values for each of the burns where no INPs were measured that would have resulted in some measureable INP signal, given the instrument backgrounds and measured N_{total} for that burn. The average ξ_{-30} values needed for the wiregrass and short African grass burns to have a measureable INP signal were −8.15 and −7.37, respectively. In comparison, averaged across the burns of the same fuel that did produce measureable N_{INP}, ξ_{-30} was −6.13 for wiregrass and −6.60 for short African grass. If the ξ_{-30} values were the same for the burns that did not have measurable N_{INP} (that is, if the aerosol was the same but simply had a lower concentration) then an INP signal would have been easily detected. Therefore, it appears that the aerosol emissions were different for the cases which did not produce INPs, even for the same fuel and same burning conditions, and not just lower in concentration. Averaged across all burns, of any fuel type, for which N_{INP} was above the detection limit, $\xi_{-30} = -7.35$. For all burns that did not emit measureable N_{INP}, an average value of −7.89 would have resulted in a measurable INP signal at the peak N_{total}. This again indicates that there was some difference in the aerosol emitted from burns that did and did not produce measureable N_{INP}.

In addition to examining which burns did or did not emit measurable N_{INP}, we also divided burns into time periods when there was or was not a measurable INP signal. These values, labeled "Times," are also shown in Figure 3. For those burns which did have measurable INP concentrations, INPs were emitted during times with, on average, higher MCE, b_{abs}, and N_{total}. Time-resolved EC/TC measurements were not available. The differences in MCE and

N_{total} were statistically significant at the 95% confidence level. The higher MCE values indicate that INPs are released during times of intense flaming combustion, as was seen in the example case shown in Figure 2. As expected, the higher MCE values during times when INPs were measured was also associated with higher b_{abs}, although the differences in b_{abs} between times with and without measureable N_{INP} was only significant at the 85% confidence level. While INP emissions were associated with flaming combustion and higher BC concentrations, it is important to note that total aerosol concentrations were also higher on average during times when INPs were measured. In fact, when the average ξ_{-30} values calculated during times when INPs were measured were applied to the N_{total} values measured when INPs were not measured, for the same burn, the resulting calculated N_{INP} values were below the measured background in almost every case. Thus, it is possible that N_{INP} were just below the detection limit during smoldering phases of combustion for the burns associated with detectable INPs.

Figure 4 shows box plots of ξ_{-30}, ranked by median ξ_{-30}, for all stack burns with measureable INP emissions. Median values are shown both before (blue) and after (red) vapor limitation correction. For clarity, box plots are only shown for the vapor limitation corrected data. The ξ_{-30} values measured during the FLAME 4 stack burns were, in general, very low compared to other known INP particle types such as Arizona Test Dust and kaolinite (as shown in Figure S1, for example). The ξ_{-30} values from FLAME 4 were also much lower than those presented by *Petters et al.* [2009] from previous FLAME measurements, even for the same fuel types, albeit from different locations [*McMeeking et al.*, 2009; *Stockwell et al.*, 2014]. *Petters et al.* [2009] had a detection limit of $\xi_{-30} > -4.6$ and measured ξ_{-30} values ranging from -4.2 to as high as -1.3 for the 9 of 21 fuels that produced particles exceeding this threshold during at least one burn. Thus, the highest INP activity measured at $-30°C$ in that study represented freezing by more than 1 out of 100 measured aerosol particles. By contrast, the highest value measured during FLAME 4 was only at the bottom of this range, $\xi_{-30} = -4$. There were, however, some important differences between the experimental setup used by *Petters et al.* [2009] and that used for this work, which may explain some of these discrepancies. During FLAME 4 we measured fire emissions that were only a few seconds old directly off of the stack, while *Petters et al.* [2009] collected emissions from the stack into a 50 gallon tank and then measured INP concentrations over a period of 15–20 min. They also processed the sample by passing it through a humidifier and subsequent dryer to collapse nonspherical fractal aggregates. This processing resulted in both aerosol losses and coagulation of smaller particles leading to a decrease in N_{total}. While INPs would also be lost via these mechanisms, smaller particles are less likely to be an INP [*DeMott et al.*, 2010]. Thus, any size-dependent aerosol loss due to coagulation could have reduced the number of N_{total} more than that of N_{INP}, leading to an increase in ξ_{-30}. Also, due to the longer sampling times, *Petters et al.* [2009] were able to scan over supersaturation in the CFDC and reported the maximum measured ξ_{-30} at roughly 9%. *DeMott et al.* [2015] showed that for mineral dust, increasing processing S_w from 5% to 9% increased N_{INP} by a factor of 3. There is evidence that this value or some correction is also valid for smoke, as *Petters et al.* [2009] also saw increases in N_{INP} for increases in S_w at least as large as those seen for mineral dust particles by *DeMott et al.* [2015]. Despite these differences, given the short lifetime of smokes at the point of sampling, and lack of any preprocessing used during FLAME 4, we consider the ξ_{-30} values presented here to be indicative of biomass burning emissions at the source. Absent the ability to perform RH scans, we can only assume no more than a factor of a few underestimate of maximum INP concentrations in the present study, after correction for vapor limitation effects. We also note that the ξ_{-30} values measured during FLAME 4 align well with those measured at the same conditions during sampling near prescribed burns and wildfires (Figure S1) [*McCluskey et al.*, 2014].

Although the ξ_{-30} values measured during FLAME 4 were low, the N_{INP} values (burn average values shown in Figure 4 both before and after vapor limitation correction) were much higher than typical ambient values [*DeMott et al.*, 2010]. Thus, biomass burning could be a contributor to INP budgets near fires due to the large number of particles released, even though only a tiny fraction of emitted particles will act as heterogeneous ice-nucleating particles. We can directly determine the contribution of biomass combustion to INP emissions by calculating emission factors, the number of INP emitted for a given amount of fuel consumed. Emission factor of INPs at $-30°C$ ($EF_{INP,-30}$) are also shown in Figure 4 as total number of INPs, corrected for vapor limitation, released per kilogram of fuel burned. We calculated the total number of INP emitted for each burn by assuming that measured INP concentrations were homogeneous across the stack profile and using an average stack flow velocity of $3.6 \, m \, s^{-1}$. We then divided this number by the fuel mass consumed during each burn to calculate emission factors. The $EF_{INP,-30}$ values are summed across the entire burn and thus include both flaming and smoldering emissions. For all burns that produced INP emissions, the median EF_{INP} at $-30°C$ was about
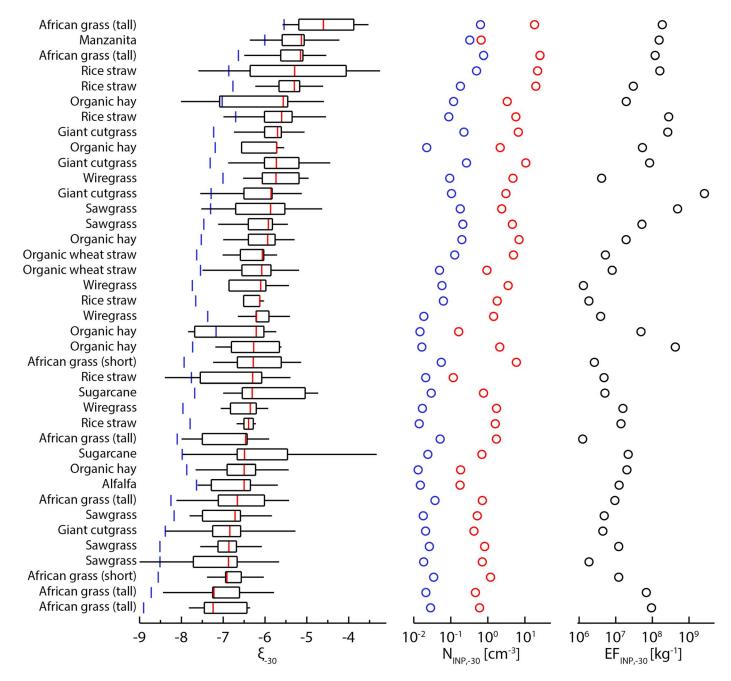
Figure 4. (left) Ice nuclei efficiency, (middle) total INP number concentration, and (right) INP emission factors for all stack burns ranked by median ice nuclei efficiency. Blue points show measured data, and red are corrected for vapor depletion. Box plots show 25th, 50th, and 75th percentiles with whiskers indicating minimum and maximum values.

$2 \times 10^7 \, kg^{-1}$. That is, each kilogram of fuel consumed by fire would release 2×10^7 ice-nucleating particles, on average. Given typical fuel mass loadings of 1–$10 \, kg \, m^{-2}$ [*Akagi et al.*, 2011; *Wiedinmyer et al.*, 2006] and the full range of $EF_{INP,-30}$ measured here, the emission factors measured during FLAME 4 translate to 1.2×10^6 to 2.7×10^{10} INP emitted per square meter burned. By comparison, *Petters et al.* [2009] estimated $EF_{INP,-30}$ values using a bottom-up approach [*Wiedinmyer et al.*, 2006] ranging from 5×10^6 to $3.4 \times 10^{15} \, m^{-2}$. These higher emissions factors are likely due to the higher ξ_{-30} values measured by *Petters et al.* [2009].

From Figure 4, it can be seen that there was little consistency in INP emissions from the different fuel types. For example, the same fuel type (tall African grass) produced both the highest and lowest median ξ_{-30}. These burns,
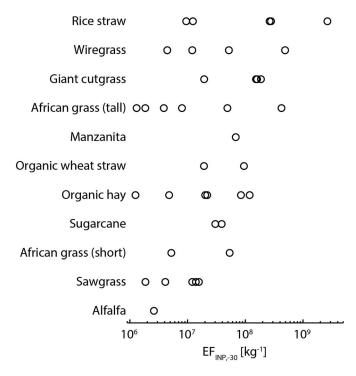
Figure 5. INP emission factors (number of INP per kilogram of fuel consumed) as a function of fuel type. Each point represents an individual stack burn. Fuels are ranked by mean EF_{INP}.

at the top and bottom of the ranking chart, used the same vertical fuel orientation as shown in Figure 2, had similar initial fuel mass, and were both lit from one edge, allowing the flame to propagate through the fuel. Figure 5 shows $EF_{INP,-30}$ by fuel type, ranked by mean $EF_{INP,-30}$. While, on average, rice straw produced the most number of INPs per kilogram consumed, the burn-to-burn variability even within the same fuel type spanned several orders of magnitude.

In addition to this lack of consistency in INP emissions within fuel types, during some single burns we measured variability in ξ_{-30} larger than the total range of median ξ_{-30} values across all burns. This large variability in ξ_{-30} observed as the burns progressed seems to indicate that burning conditions, not fuel type, may play a larger role in determining ξ_{-30}, as well as the EF_{INP}, of the emitted aerosol. However, while burn conditions appear to be important for INP production and INPs were preferentially measured from burns with higher overall MCE values, as shown above, there was little relation between MCE and ξ_{-30} (Figure 6). Only five burns (colored points in Figure 6) had correlation coefficients (r^2) between MCE and ξ_{-30} of 0.5 or higher. Averaged across all the other burns (gray points in Figure 6), the r^2 value between MCE and ξ_{-30} was only 0.1. Further, over all burns, the average r^2 value between burn median ξ_{-30} and burn median MCE was only 0.1, indicating no correlation between the two variables. Likewise, the r^2 value between $EF_{INP,-30}$ and burn median MCE was 0.02. There are several possible reasons why MCE may not be a good predictor of INP emissions. For example, carbonaceous aerosol emissions can vary widely for the same MCE values. Black carbon yield from flaming combustion is variable and responds to factors other than combustion efficiency, such as turbulence. Even a gentle breeze can increase BC yield by a factor of ~10 [*Shaddix et al.*, 1994]. Also, smoldering combustion consists of two processes; "glowing" and "pyrolysis." While both have low MCE, only pyrolysis produces organic aerosol (OA), and thus, the glowing/pyrolysis ratio and OA emissions can vary without associated large changes in MCE [*Yokelson et al.*, 1996; *Yokelson et al.*, 1997]. Further, the problem with this type of analysis is that we are attempting to explain a very small fraction of the total aerosol emissions, typically one in a million of the emitted particles or fewer, with bulk fire properties. Thus, while it appears that INP were emitted during flaming combustion and thus it is possible that BC particles contributed to the INP population, this analysis alone is insufficient to draw such conclusions. Therefore, during the room burn experiments we directly measured the contribution of black carbon particles to INP concentrations.
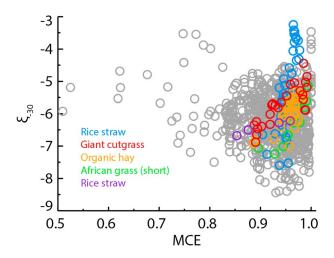
Figure 6. Ice nuclei efficiency versus modified combustion efficiency for all stack burns. Colors indicate burns with correlation coefficient (r^2) > 0.5 with different colors indicating different burns.

3.2. Room Burns

We collected data with the CFDC during 16 room burns. These fires were similar in size and burn characteristics to the stack burns, but the smoke was held in the combustion lab for 2–4 h. We thus sampled well mixed, total fire emissions during these tests instead of the real-time emissions as the fire progressed, as was done during stack burns. For all experiments we waited 15 min after ignition to allow fire emissions to become well mixed in the room before we began measurements. The extended sampling time for these experiments allowed us to measure at more than one CFDC processing temperature as well as sample with the SP2-CFDC setup.

During the room burn experiments, we measured increases in INP concentrations above instrument background during all but one burn (Table 1). Only the peat fuel, which burned with smoldering combustion only and had a burn averaged MCE of 0.8, did not produce detectable INPs. Unlike the stack burns, we did measure increases in N_{INP} during three Ponderosa pine room burns, all of which had intense flaming phases at the beginning of the burn. We also measured INP emissions from black spruce during the room burns, which we were unable to measure during the stack burn experiments.
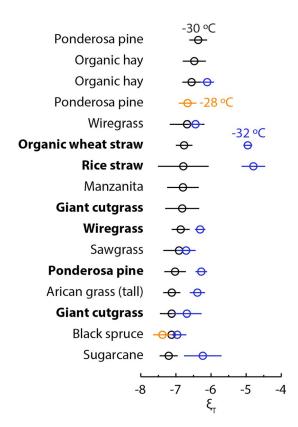

Figure 7. Mean and standard deviation ice-nucleating efficiency for room burns at −28°C (orange), −30°C (black), and −32°C (blue). Bold lettering indicates burns for which SP2-CFDC measurements were made (Figure 10).

Figure 7 shows the mean ξ_T values (±1 standard deviation) for the room burns. These values are all corrected in the same manner as the stack burns for vapor limitation, although given the lower aerosol loadings during these burns there was less correction in ξ_T. Unlike the box plots shown for the stack burns, these data do not show the time-varying range in ξ_T emitted by the fire, just the variability of the mixed smoke during the measurement periods. As can also be seen in Figure 7, the longer sampling period during room burns allowed for measurements at -28°C for two burns, and for many burns we also measured at −32°C. Decreasing processing temperature led to an increase in N_{INP} in every case, although with some variability in the increases. Averaged across all burns, decreasing processing temperature from −30°C to −32°C led to an 11% increase in ξ_T. While this shows the importance of processing temperature to INP activity for biomass combustion emissions, to fully parameterize biomass burning INP temperature dependence, measurements need to be
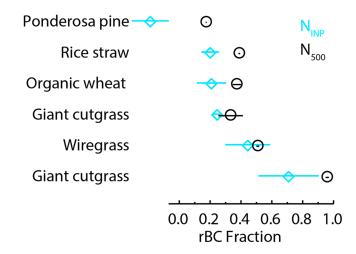
Figure 8. Refractory black carbon fractions of N_{500} (black) and N_{INP} (blue) determined from SP2-CFDC measurements.

performed across a broader temperature range. The bold fuel names in Figure 7 indicate the burns for which we were able to measure with the SP2-CFDC setup.

3.2.1. SP2-CFDC

While the stack burn experiments suggested that INPs were emitted during intense flaming combustion, when BC emissions were higher, we have no way to confirm if BC particles were responsible for ice nucleation from these data alone. During the room burns, we were able to directly address the question of whether black carbon particles contributed to the INP population emitted from biomass combustion by utilizing the SP2-CFDC technique described by *Levin et al.* [2014]. For these experiments, sample was first passed through the SP2 and then the SP2 exhaust was sent to the CFDC. Since refractory black carbon (rBC) particles larger than ~100 nm in diameter are removed by the SP2 laser via laser-induced vaporization, while nonabsorbing material will pass through the laser unchanged, by switching between SP2 laser on and off, we were able to determine the contribution of rBC particles to N_{500} and N_{INP}. We assume that any decrease in measured N_{500} or N_{INP} when the laser was turned on was due to the removal of rBC, since no other variable in the sampling system was changed, and thus term this the rBC fraction. We also assume that for any coated rBC particle, it is the insoluble rBC core that is responsible for ice nucleation and thus will refer to these as rBC INP and not rBC-containing INP. For N_{500}, however, the particles removed by the laser could contain an rBC core smaller than 500 nm coated with some other aerosol component and thus these should be considered rBC-containing particles. During the FLAME 4 room burns, data were collected with the laser on and off for about 3 min each with 1 min between samples and typically for two on/off cycles for each burn. Data were averaged over each sampling period, and then we linearly fit the laser on and laser off data and compared the ratio between fits to determine the rBC fraction [*Levin et al.*, 2014].

Figure 8 shows the results of the SP2-CFDC tests plotted as the rBC fraction of N_{500} and N_{INP}. Burns are ranked from the lowest to highest contribution of rBC to N_{INP}. The error bars represent variability calculated from the standard error of the mean during the averaging period. Laser processing led to a decrease in aerosol and INP concentrations in almost every case, thus indicating that some rBC particles were present in the aerosol population above 500 nm and as INPs. There was considerable variability in the rBC fractions for both N_{INP} and N_{500} across burns with values for the rBC fraction of N_{500} ranging from 0.17 to 0.96 and for N_{INP} from 0 to 0.7. It is interesting that while INPs were released during intense flaming combustion for the Ponderosa pine burn, and not during the smoldering combustion case of the stack burns, there was no contribution from rBC to the INP population for this burn. Thus, these data also indicate that fires emit non-rBC INPs, and in the case of the Ponderosa pine burn these other INP types were dominant. For certain common grass fuels, however, rBC was the largest INP particle type.

While the rBC fractions for N_{500} and N_{INP} were variable from burn to burn, even for the same fuel type, there was considerable consistency between the two fractions with an r^2 value of 0.87 (Figure 9). Previous studies have shown correlations between INP number concentrations and number concentrations of particles above 500 nm [*DeMott et al.*, 2010]. The good correlation between the rBC fractions of N_{INP} and N_{500} suggest that the
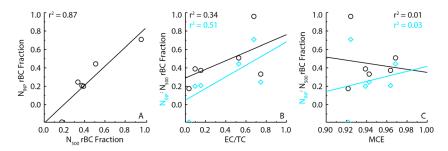
Figure 9. (a) Refractory black carbon (rBC) fractions of N_{INP} versus rBC fractions of N_{500}, (b) rBC fractions of N_{INP} and N_{500} versus EC to TC ratios, and (c) rBC fractions of N_{INP} and N_{500} versus MCE.

rBC-associated INPs measured during the FLAME 4 burns extended into the size range above 500 nm, such that particle number concentrations larger than 500 nm provide a good predictor for rBC INP. We also plotted the rBC fractions shown in Figure 8 against the EC/TC ratio from $PM_{2.5}$ filters and burn-averaged MCE (Figure 9). The correlations between rBC fractions determined from the SP2-CFDC and EC/TC from filter analysis was weak with r^2 values of 0.34 and 0.51 for N_{500} and N_{INP}, respectively. However, it is important to note that these measurements are comparing number and mass ratios and the size ranges are not identical. There was no correlation between MCE and the rBC fractions of either N_{500} or N_{INP}. As noted above, it is not surprising that INPs, which account for a tiny fraction of the total aerosol, do not correlate with bulk fire properties. Also, while previous studies have shown correlations between MCE and BC fractions [*McMeeking et al.*, 2009] the relationship tends to be weak at high MCE values, as was the case for these burns, and BC emissions can be influenced by other factors [*Shaddix et al.*, 1994].

We can directly assess the efficacy of the SP2-CFDC technique to determine the contribution of rBC to the INP population by comparing these results to those from scanning electron microscopy and energy dispersive X-ray (SEM/EDX) analyses of the CFDC-activated ice crystal residuals, as was done by *McCluskey et al.* [2014]. For the wiregrass burn shown in Figure 8, we have data from such analysis as well as the SP2-CFDC results. Figure 10 shows example SEM images from 54 ice crystal residuals which were analyzed from this burn. The SEM grid was collected immediately before sampling through the SP2 and should thus represent the particle types measured with the SP2-CFDC setup. Of the particles examined, 44% were identified as soot, as evidenced by their fractal morphology and carbon-dominated elemental composition. Another 4% of particles were classified as soot with organic inclusions, which appeared to be tarballs [*Posfai et al.*, 2004]. The remaining 52% of the residual INPs (labeled "other" in Figure 10) contained no obvious soot and appeared to be plant fragments or secondary organic species, such as tarballs. The fraction of soot or soot-containing INPs from the SEM analysis agreed very well with that determined by the SP2-CFDC for this burn, further validating the use of this method. Also, the SEM analysis showed only a small number of cases of soot particles mixed with other nonvolatile aerosol types, which could potentially complicate the SP2-CFDC analysis [*Levin et al.*, 2014]. While we only have overlapping SEM and SP2-CFDC data for one FLAME 4 burn, *McCluskey et al.* [2014] collected and analyzed ice crystal residuals from wildfires and prescribed burns dominated by Ponderosa pine and wiregrass fuels, respectively, and compared their results to those from similar fuels burned during FLAME 4. As previously reported in their work, for the wiregrass-dominated prescribed burns, they observed soot fractions between 0.33 and 0.66 and did not find any soot-containing ice crystal residuals
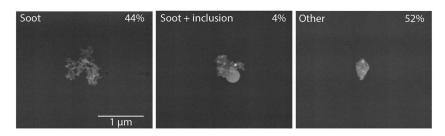

Figure 10. Example SEM images showing ice crystal residuals from a room burn with wiregrass. All residuals ($n = 54$) were identified as one of the three shown classes.

for the wildfires dominated by Ponderosa pine. Both of these results are in very good agreement with the rBC fractions found using the SP2-CFDC setup on similar fuels burned during FLAME 4.

4. Conclusions

FLAME 4 provided a unique opportunity to measure emissions from biomass combustion directly at the source as fires progressed from ignition to extinction. The fuels burned represented globally relevant fuels often consumed during wildfires, prescribed burns, and agricultural burning. Of all fuels tested, 13 of 22 produced some measureable INP emissions during at least one burn. Burns that did not produce measureable INPs had, on average, lower total aerosol concentrations, lower MCE values, lower black carbon concentrations, and a lower EC to TC ratios. It was also observed that for burns which produced INPs, emissions were strongest during times of intense flaming combustion. These results suggest that black carbon accounts for at least some of the INPs emitted by biomass combustion in many cases.

The ice nuclei efficiency (ξ_{-30}) of emitted aerosol, the fraction of particles capable of heterogeneous ice nucleation at $-30°C$, was typically very low compared to other known ice-nucleating aerosol types but agreed well with measurements made near prescribed burns and wildfires. Ice nuclei efficiency and INP emission factors were also highly variable across burns, even for the same fuel type, and ξ_{-30} showed large variability within individual burns. This is likely due to the complex nature of biomass combustion and the variability of emitted aerosol size, composition, and mixing state. Further, INPs accounted for, on average, about one in a million of the emitted aerosol particles, thus making it hard to reliably relate their characteristics to those of bulk emissions.

During a second set of experiments, total fire emissions were held in a closed room for several hours, allowing for extended analysis time. During these burns, we directly investigated the contribution of refractory black carbon (rBC) aerosol to INP emissions by selectively removing these particles via laser-induced incandescence and measuring the change in N_{INP} as well as N_{500}. These experiments showed that rBC particles accounted for 0–70% of the emitted INPs, with only one case showing no decrease in N_{INP} when rBC was removed. Furthermore, the INP rBC fractions determined from SP2-CFDC analysis agreed very well with SEM analysis of collected ice crystal residuals for one FLAME 4 test case as well as INP collected during prescribed burns and wildfires of similar fuels, wiregrass, and Ponderosa pine [*McCluskey et al.*, 2014]. This good comparison further validates this new measurement technique, at least for the fuels where similar inspection was done.

Overall, the FLAME 4 study showed that fires can be an important source of heterogeneous ice nuclei, although the ice nucleation efficiency of emitted aerosols are lower than other known INP types. Further, these experiments illustrated that soot, or refractory black carbon, aerosol contributes to the INP population emitted from fires and, in some cases, can be the dominant ice-nucleating aerosol type.

References

Aiken, A. C., G. R. McMeeking, M. K. Dubey, P. J. DeMott, E. J. T. Levin, and S. M. Kreidenweis (2016), Online removal of submicron refractory black carbon using laser-induced incandescence in the single particle soot photometer: Efficacy and application with Aquadag, *Aerosol Sci. Technol.*, doi:10.1080/02786826.2016.1173647.

Akagi, S. K., R. J. Yokelson, C. Wiedinmyer, M. J. Alvarado, J. S. Reid, T. Karl, J. D. Crounse, and P. O. Wennberg (2011), Emission factors for open and domestic biomass burning for use in atmospheric models, *Atmos. Chem. Phys.*, *11*(9), 4039–4072, doi:10.5194/acp-11-4039-2011.

Arnott, W. P., H. Moosmuller, C. F. Rogers, T. F. Jin, and R. Bruch (1999), Photoacoustic spectrometer for measuring light absorption by aerosol: Instrument description, *Atmos. Environ.*, *33*(17), 2845–2852.

Bond, T. C., et al. (2013), Bounding the role of black carbon in the climate system: A scientific assessment, *J. Geophys. Res. Atmos.*, *118*, 5380–5552, doi:10.1002/jgrd.50171.

Chow, J. C., J. G. Watson, L. W. A. Chen, M. C. O. Chang, N. F. Robinson, D. Trimble, and S. Kohl (2007), The IMPROVE-A temperature protocol for thermal/optical carbon analysis: Maintaining consistency with a long-term database, *J. Air Waste Manage.*, *57*(9), 1014–1023, doi:10.3155/1047-3289.57.9.1014.

Christian, T. J., B. Kleiss, R. J. Yokelson, R. Holzinger, P. J. Crutzen, W. M. Hao, T. Shirai, and D. R. Blake (2004), Comprehensive laboratory measurements of biomass-burning emissions: 2. First intercomparison of open-path FTIR, PTR-MS, and GC- MS/FID/ECD, *J. Geophys. Res.*, *109*, D02311, doi:10.1029/2003JD003874.

DeMott, P. J. (1990), An exploratory-study of ice nucleation by soot aerosols, *J. Appl. Meteorol.*, *29*(10), 1072–1079, doi:10.1175/1520-0450(1990)029<1072:aesoin>2.0.co;2.

DeMott, P. J., A. J. Prenni, X. Liu, S. M. Kreidenweis, M. D. Petters, C. H. Twohy, M. S. Richardson, T. Eidhammer, and D. C. Rogers (2010), Predicting global atmospheric ice nuclei distributions and their impacts on climate, *Proc. Natl. Acad. Sci. U.S.A.*, *107*(25), 11,217–11,222, doi:10.1073/pnas.0910818107.

DeMott, P. J., et al. (2015), Integrating laboratory and field data to quantify the immersion freezing ice nucleation activity of mineral dust particles, *Atmos. Chem. Phys.*, *15*(1), 393–409, doi:10.5194/acp-15-393-2015.

Diehl, K., and S. K. Mitra (1998), A laboratory study of the effects of a kerosene-burner exhaust on ice nucleation and the evaporation rate of ice crystals, *Atmos. Environ.*, *32*(18), 3145–3151, doi:10.1016/s1352-2310(97)00467-6.

Gorbunov, B., A. Baklanov, N. Kakutkina, H. L. Windsor, and R. Toumi (2001), Ice nucleation on soot particles, *J. Aerosol Sci.*, *32*(2), 199–215, doi:10.1016/s0021-8502(00)00077-x.

Hoose, C., and O. Moehler (2012), Heterogeneous ice nucleation on atmospheric aerosols: A review of results from laboratory experiments, *Atmos. Chem. Phys.*, *12*(20), 9817–9854, doi:10.5194/acp-12-9817-2012.

Levin, E. J. T., et al. (2010), Biomass burning smoke aerosol properties measured during Fire Laboratory at Missoula Experiments (FLAME), *J. Geophys. Res.*, *115*, D18210, doi:10.1029/2009JD013601.

Levin, E. J. T., G. R. McMeeking, P. J. DeMott, C. S. McCluskey, C. E. Stockwell, R. J. Yokelson, and S. M. Kreidenweis (2014), A new method to determine the number concentrations of refractory black carbon ice nucleating particles, *Aerosol Sci. Technol.*, *48*(12), 1264–1275, doi:10.1080/02786826.2014.977843.

Levin, M., A. Gudmundsson, J. H. Pagels, M. Fierz, K. Molhave, J. Londahl, K. A. Jensen, and I. K. Koponen (2015), Limitations in the use of unipolar charging for electrical mobility sizing instruments: A study of the fast mobility particle sizer, *Aerosol Sci. Technol.*, *49*(8), 556–565, doi:10.1080/02786826.2015.1052039.

Levin, Z., and W. R. Cotton (2009), *Aerosol Pollution Impact on Precipitation: A Scientific Review*, 1 pp., online resource (xxi, 386 p.) ill. (some col.), maps, Springer, Dordrecht, London.

Lu, Z., and I. N. Sokolik (2013), The effect of smoke emission amount on changes in cloud properties and precipitation: A case study of Canadian boreal wildfires of 2007, *J. Geophys. Res. Atmos.*, *118*, 11,777–11,793, doi:10.1002/2013JD019860.

McCluskey, C. S., P. J. DeMott, A. J. Prenni, E. J. T. Levin, G. R. McMeeking, A. P. Sullivan, T. C. J. Hill, S. Nakao, C. M. Carrico, and S. M. Kreidenweis (2014), Characteristics of atmospheric ice nucleating particles associated with biomass burning in the US: Prescribed burns and wildfires, *J. Geophys. Res. Atmos.*, *119*, 10,458–10,470, doi:10.1002/2014JD021980.

McMeeking, G. R., et al. (2009), Emissions of trace gases and aerosols during the open combustion of biomass in the laboratory, *J. Geophys. Res.*, *114*, D19210, doi:10.1029/2009JD011836.

Murray, B. J., D. O'Sullivan, J. D. Atkinson, and M. E. Webb (2012), Ice nucleation by particles immersed in supercooled cloud droplets, *Chem. Soc. Rev.*, *41*(19), 6519–6554, doi:10.1039/c2cs35200a.

Nakayama, T., H. Suzuki, S. Kagamitani, Y. Ikeda, A. Uchiyama, and Y. Matsumi (2015), Characterization of a three wavelength Photoacoustic Soot Spectrometer (PASS-3) and a Photoacoustic Extinctiometer (PAX), *J. Meteorol. Soc. Jpn.*, *93*(2), 285–308, doi:10.2151/jmsj.2015-016.

Petters, M. D., et al. (2009), Ice nuclei emissions from biomass burning, *J. Geophys. Res.*, *114*, D07209, doi:10.1029/2008JD011532.

Petzold, A., et al. (2013), Recommendations for reporting "black carbon" measurements, *Atmos. Chem. Phys.*, *13*(16), 8365–8379, doi:10.5194/acp-13-8365-2013.

Posfai, M., A. Gelencser, R. Simonics, K. Arato, J. Li, P. V. Hobbs, and P. R. Buseck (2004), Atmospheric tar balls: Particles from biomass and biofuel burning, *J. Geophys. Res.*, *109*, D06213, doi:10.1029/2003JD004169.

Prenni, A. J., P. J. DeMott, A. P. Sullivan, R. C. Sullivan, S. M. Kreidenweis, and D. C. Rogers (2012), Biomass burning as a potential source for atmospheric ice nuclei: Western wildfires and prescribed burns, *Geophys. Res. Lett.*, *39*, L11805, doi:10.1029/2012GL051915.

Reid, J. S., R. Koppmann, T. F. Eck, and D. P. Eleuterio (2005), A review of biomass burning emissions part II: Intensive physical properties of biomass burning particles, *Atmos. Chem. Phys.*, *5*, 799–825.

Rogers, D. C. (1988), Development of a continuous flow thermal gradient diffusion chamber for ice nucleation studies, *Atmos. Res.*, *22*, 149–181.

Rogers, D. C., P. J. DeMott, S. M. Kreidenweis, and Y. L. Chen (2001), A continuous-flow diffusion chamber for airborne measurements of ice nuclei, *J. Atmos. Oceanic Technol.*, *18*(5), 725–741, doi:10.1175/1520-0426(2001)018<0725:acfdcf>2.0.co;2.

Sassen, K., and V. I. Khvorostyanov (2008), Cloud effects from boreal forest fire smoke: Evidence for ice nucleation from polarization lidar data and cloud model simulations, *Environ. Res. Lett.*, *3*(2), doi:10.1088/1748-9326/3/2/025006.

Shaddix, C. R., J. E. Harrington, and K. C. Smyth (1994), Quantitative measurements of enhanced soot production in a flickering methane air diffusion flame, *Combust. Flame*, *99*(3–4), 723–732, doi:10.1016/0010-2180(94)90067-1.

Stockwell, C. E., R. J. Yokelson, S. M. Kreidenweis, A. L. Robinson, P. J. DeMott, R. C. Sullivan, J. Reardon, K. C. Ryan, D. W. T. Griffith, and L. Stevens (2014), Trace gas emissions from combustion of peat, crop residue, domestic biofuels, grasses, and other fuels: Configuration and Fourier transform infrared (FTIR) component of the fourth Fire Lab at Missoula Experiment (FLAME-4), *Atmos. Chem. Phys.*, *14*(18), 9727–9754, doi:10.5194/acp-14-9727-2014.

Twohy, C. H., et al. (2010), Relationships of biomass-burning aerosols to ice in orographic wave clouds, *J. Atmos. Sci.*, *67*(8), 2437–2450, doi:10.1175/2010jas3310.1.

Umo, N. S., B. J. Murray, M. T. Baeza-Romero, J. M. Jones, A. R. Lea-Langton, T. L. Malkin, D. O'Sullivan, L. Neve, J. M. C. Plane, and A. Williams (2015), Ice nucleation by combustion ash particles at conditions relevant to mixed-phase clouds, *Atmos. Chem. Phys.*, *15*(9), 5195–5210, doi:10.5194/acp-15-5195-2015.

Vali, G., P. J. DeMott, O. Mohler, and T. F. Whale (2015), Technical note: A proposal for ice nucleation terminology, *Atmos. Chem. Phys.*, *15*(18), 10,263–10,270, doi:10.5194/acp-15-10263-2015.

Wiedinmyer, C., B. Quayle, C. Geron, A. Belote, D. McKenzie, X. Zhang, S. O'Neill, and K. K. Wynne (2006), Estimating emissions from fires in North America for air quality modeling, *Atmos. Environ.*, *40*(19), 3419–3432, doi:10.1016/j.atmosenv.2006.02.010.

Yokelson, R. J., D. W. T. Griffith, and D. E. Ward (1996), Open-path Fourier transform infrared studies of large-scale laboratory biomass fires, *J. Geophys. Res.*, *101*(D15), 21,067–21,080, doi:10.1029/96JD01800.

Yokelson, R. J., R. Susott, D. E. Ward, J. Reardon, and D. W. T. Griffith (1997), Emissions from smoldering combustion of biomass measured by open-path Fourier transform infrared spectroscopy, *J. Geophys. Res.*, *102*(D15), 18,865–18,877, doi:10.1029/97JD00852.

Yokelson, R. J., T. J. Christian, T. G. Karl, and A. Guenther (2008), The tropical forest and fire emissions experiment: Laboratory fire measurements and synthesis of campaign data, *Atmos. Chem. Phys.*, *8*(13), 3509–3527.